

Non- d^0 Electric Dipole in FeO_5 bipyramid: a New Resource for Quantum Paraelectrics, Ferroelectrics and Multiferroics

Shi-Peng Shen, Yi-Sheng Chai,* Jun-Zhuang Cong, Pei-Jie Sun, Jun Lu, Li-Qin Yan,
Shou-Guo Wang, and Young Sun†

Beijing National Laboratory for Condensed Matter Physics, Institute of Physics,

Chinese Academy of Sciences, Beijing 100190, China

*yschai@iphy.ac.cn †youngsun@iphy.ac.cn

Abstract

Electric polarization in conventional ferroelectric oxides usually involves nonmagnetic transition-metal ions with an empty d shell (the d^0 rule). Here we unravel a new mechanism for local electric dipoles based on magnetic Fe^{3+} ($3d^5$) ion violating the d^0 rule. The competition between the long-range Coulomb interaction and short-range Pauli repulsion in a FeO_5 bipyramid with proper lattice parameters would favor an off-center displacement of Fe^{3+} that induces a local electric dipole. The manipulation of this kind of non- d^0 electric dipoles opens up a new route for generating unconventional dielectrics, ferroelectrics, and multiferroics. As a prototype example, we show that the non- d^0 electric dipoles in ferrimagnetic hexaferrites $(\text{Ba,Sr})\text{Fe}_{12}\text{O}_{19}$ lead to a new family of magnetic quantum paraelectrics.

The majority of conventional ferroelectrics are transitional metal oxides with a perovskite structure (ABO_3) such as $BaTiO_3$ and $(Pb,Zr)TiO_3$. Their electric polarization usually requires an off-center shifting of transition metal (B) ions with an empty d shell due to the hybridization between empty d orbital and filled O $2p$ orbitals [1, 2]. This empirical “ d^0 rule” established by Matthias [3] has severely restrained the family of ferroelectrics and even precludes the coexistence of electric and magnetic orders because magnetism normally requires non- d^0 configurations [4]. In order to incorporate ferroelectricity with magnetism, other mechanisms of ferroelectricity without involving the B -site off-centering for electric polarization, such as A -site lone-pair electrons [5], non-collinear spin configurations [6], charge ordering [7,8], and geometric ferroelectricity [9], have been extensively studied in the past decade.

On the other hand, recent studies suggest that the d^0 rule could be broken in certain circumstances. For example, theoretical calculations predicted the possible ferroelectricity in $AMnO_3$ ($A=Sr, Ca, \text{ and } Ba$) driven by off-centering of the magnetic Mn^{4+} ion in MnO_6 octahedron via the second-order Jahn-Teller effect [10-12]. Recently, ferroelectricity was indeed observed in perovskite $Sr_{1-x}Ba_xMnO_3$ ($x \geq 0.45$) single crystals [13]. This progress poses a big challenge to the empirical d^0 rule. In this Letter, we demonstrate another intriguing case violating the d^0 rule other than the perovskite oxides. It is found that the delicate balance between the long-range Coulomb interaction and short-range Pauli repulsion in a FeO_5 bipyramid would favor an off-center displacement of the magnetic Fe^{3+} ions, which directly induces a local electric dipole.

This type of non- d^0 electric dipole provides a new resource for unconventional dielectrics, ferroelectrics, and multiferroics.

The principle unraveled in this work initially originates from the understanding of the abnormal dielectric behaviors in the M-type hexaferrites $(\text{Ba,Sr})\text{Fe}_{12}\text{O}_{19}$. Hexaferrites are iron oxides with hexagonal structures. Depending on their chemical formula and crystal structures, hexaferrites can be classified into several types [14,15]: M-type $(\text{Ba,Sr})\text{Fe}_{12}\text{O}_{19}$, Y-type $(\text{Ba,Sr})_2\text{Me}_2\text{Fe}_{12}\text{O}_{22}$, W-type $(\text{Ba,Sr})\text{Me}_2\text{Fe}_{16}\text{O}_{27}$, X-type $(\text{Ba,Sr})_2\text{Me}_2\text{Fe}_{28}\text{O}_{46}$, Z-type $(\text{Ba,Sr})_3\text{Me}_2\text{Fe}_{24}\text{O}_{41}$, and U-type $(\text{Ba,Sr})_4\text{Me}_2\text{Fe}_{36}\text{O}_{60}$, where Me = a bivalent metal ion. As shown in Fig. 1, the structures of hexaferrites can be described by a periodically stacking sequence of three basic building blocks (S, R, and T blocks) along c axis. The Fe^{3+} ions occupy three different kinds of sites: octahedral, tetrahedral, and bipyramidal sites. In particular, the FeO_5 bipyramids only exist in the middle of R blocks where the equatorial plane of the bipyramid is a mirror plane. Among all the hexaferrites, the M-type hexaferrites have the simplest crystal structure, consisting of alternate stacks of S and R blocks along c axis. Both $\text{BaFe}_{12}\text{O}_{19}$ and $\text{SrFe}_{12}\text{O}_{19}$ have a collinear ferrimagnetic ordering along c axis, with a Neel temperature of ~ 720 [16] and 737 K [17], respectively. This spin configuration persists down to the lowest temperature without any magnetic transition.

We have prepared various single-crystal and polycrystalline samples of hexaferrites to investigate their dielectric properties. The details of sample preparation and characterization are given in the Supplementary Material [18]. The dielectric permittivity

was measured using an Agilent 4980A LCR meter at 1 MHz in a Cryogen-free Superconducting Magnet System (Oxford Instruments, TeslatronPT). Specific heat measurement was performed in a Quantum Design Physical Properties Measurement System.

As shown in Fig. 2(a), the c -axis dielectric permittivity $\varepsilon_c(T)$ of BaFe₁₂O₁₉ increases steadily with decreasing temperature and remains nearly constant below ~ 5.5 K. This saturation behavior in dielectric permittivity resembles well that of quantum paraelectrics such as SrTiO₃ [19], CaTiO₃ [20], and KTaO₃ [21], where the onset of ferroelectric order is suppressed by quantum fluctuations. While the Curie-Weiss law describes well the paraelectric $\varepsilon(T)$ at high temperatures, it fails in the region of a quantum paraelectric state. Instead, the mean-field Barret formula [22] is often used to describe the $\varepsilon(T)$ of quantum paraelectrics in the entire temperature region:

$$\varepsilon = \varepsilon_0 + \frac{M}{\left(\frac{1}{2}T_1\right) \coth\left(\frac{T_1}{2T}\right) - T_0} \quad (1)$$

where ε_0 is a constant, T_0 is proportional to the effective dipole-dipole coupling constant and the positive and negative values correspond to ferro and antiferroelectric interactions, respectively. T_1 represents the tunneling integral and is a dividing temperature between the low temperature region where quantum fluctuation is important and the high temperature region where quantum effect is negligible. $M = n\mu^2/k_B$, where n is the density of dipoles and μ denotes the local dipolar moment.

We find that the $\varepsilon_c(T)$ of BaFe₁₂O₁₉ can be well fitted by Eq. (1) in the entire

temperature region. The parameters obtained from the fitting curve are listed in Table I. The negative value of $T_0 = -11.7$ K implies an antiferroelectric coupling between electric dipoles. The value of $T_1 = 54.9$ K is comparable to that of SrTiO_3 , but $M = 452$ K is two orders of magnitude smaller than that of SrTiO_3 . We note that this quantum paraelectric behavior is observable only along c axis. As shown in Fig. 2(b) for comparison, the ab -plane dielectric permittivity measured along the $[100]$ direction decreases monotonically with decreasing temperature. This result suggests that the electric dipoles in $\text{BaFe}_{12}\text{O}_{19}$ are along c axis. To further verify that the saturation of ϵ_c at low temperatures has nothing to do with any phase transition, we measured the specific heat C_p of $\text{BaFe}_{12}\text{O}_{19}$ down to 2 K. No anomaly due to a phase transition could be detected (see the Supplementary Material [18]). Therefore, $\text{BaFe}_{12}\text{O}_{19}$ is a distinctive quantum paraelectric with a hexagonal structure, in contrast to those well-known perovskite quantum paraelectrics.

We then checked the consequence of Sr doping on the quantum paraelectricity. As shown in Figs. 2(c) and 2(d), both $\text{Ba}_{0.5}\text{Sr}_{0.5}\text{Fe}_{12}\text{O}_{19}$ and $\text{SrFe}_{12}\text{O}_{19}$ also exhibit quantum paraelectric behavior in the $\epsilon_c(T)$. Especially, the plateau in $\epsilon_c(T)$ extends to higher temperatures with higher Sr content, indicating that Sr doping actually enhances quantum fluctuations. The fitting parameters of Eq. (1) to both $\epsilon_c(T)$ curves indeed give a larger T_1 in $\text{Ba}_{0.5}\text{Sr}_{0.5}\text{Fe}_{12}\text{O}_{19}$ than that in $\text{BaFe}_{12}\text{O}_{19}$ (Table I). Besides, Sr doping reduces the magnitude of both T_0 and M , indicating a weaker effective dipole-dipole coupling and a smaller local dipole moment in $\text{Ba}_{0.5}\text{Sr}_{0.5}\text{Fe}_{12}\text{O}_{19}$. Note that, there is a relatively large ϵ_c

(T) background above 100 K in $\text{SrFe}_{12}\text{O}_{19}$, due to the rise of conductivity at high temperatures. Therefore, the fitting parameters of T_0 and T_1 for $\text{SrFe}_{12}\text{O}_{19}$ are not reliable while the parameter M is not so sensitive to the high temperature background to lose physical meaning. In this sense, we are safe to say that the local dipole moment is suppressed by Sr doping.

The above results reveal that all the members of $(\text{Ba,Sr})\text{Fe}_{12}\text{O}_{19}$ are quantum paraelectrics. As they also have a ferrimagnetic ground state, $(\text{Ba,Sr})\text{Fe}_{12}\text{O}_{19}$ represents a new family of magnetic quantum paraelectrics. Since the first discovery of quantum paraelectricity in SrTiO_3 by Müller *et al.* in 1979 [19], magnetic quantum paraelectrics where quantum paraelectricity coexists with magnetic ordering have been rarely observed. The only known example so far is EuTiO_3 that exhibits quantum paraelectricity along with an antiferromagnetic order [23]. The $(\text{Ba,Sr})\text{Fe}_{12}\text{O}_{19}$ family is the first example of ferrimagnetic quantum paraelectrics ever known.

To understand the physical mechanism underlying the magnetic quantum paraelectricity in $(\text{Ba,Sr})\text{Fe}_{12}\text{O}_{19}$, we need to find out the origin of local electric dipoles first. As seen in Fig. 1, the structure of $(\text{Ba,Sr})\text{Fe}_{12}\text{O}_{19}$ consists of alternating R and S blocks. The FeO_5 bipyramids residing in the middle of the R blocks, if in the centrosymmetric structure with space group $\text{P6}_3/\text{mmc}$, would not generate local electric dipoles. However, some experiments [24,25] have suggested the existence of off-equatorial displacements of Fe^{3+} at Wyckoff position of 2b site, which results in two adjacent Wyckoff positions of 4e sites with a lowered symmetry. If the off-equatorial

displaced Fe^{3+} at the 4e sites has a lower energy than the high symmetric 2b sites, a local electric dipole P along c axis would be favored, as illustrated in Fig. 3(a). Therefore, the highly anisotropic displacements of Fe^{3+} at 4e sites could be the origin of the local dipoles we are looking for. Moreover, the parameter M is found to decrease systematically with Sr doping (Table I). From the fitted M values and the nominal density of 4e sites, $n = 2.86 \times 10^{27} \text{ m}^{-3}$, the local dipole moments $\mu = 0.68, 0.50, \text{ and } 0.09 \text{ e}\text{\AA}$ are obtained for $\text{BaFe}_{12}\text{O}_{19}$, $\text{Ba}_{0.5}\text{Sr}_{0.5}\text{Fe}_{12}\text{O}_{19}$, and $\text{SrFe}_{12}\text{O}_{19}$, respectively. The decreasing dipole moment with increasing Sr content suggests a smaller off-equatorial displacements for the 4e sites, which is consistent with the x-ray refinement results [24,26] that the 4e-4e distance at room temperature decreases from $0.34(1) \text{ \AA}$ to $0.194(10) \text{ \AA}$ from $\text{BaFe}_{12}\text{O}_{19}$ to $\text{SrFe}_{12}\text{O}_{19}$. Mössbauer study [27] also revealed a similar tendency at 4.2 K that the 4e-4e distances are $0.176(5)$ and 0.133 for $\text{BaFe}_{12}\text{O}_{19}$ and $\text{SrFe}_{12}\text{O}_{19}$, respectively.

To give a more convincing assessment to the origin of local dipoles, we did theoretical simulations on the local potential energy profiles along c axis within the FeO_5 bipyramid for $(\text{Ba,Sr})\text{Fe}_{12}\text{O}_{19}$. We adopted a phenomenological local potential energy of the following form for the bipyramid [28]:

$$U_{\text{tot}}(z) = U_{\text{Coulomb}}(z) + U_{\text{repulsion}}(z) = -\frac{3 \times 6e^2}{\sqrt{r_0^2 + z^2}} - \frac{6e^2}{r_1 + z} - \frac{6e^2}{r_1 - z} + 3\beta_{c+-} e^{(r_+ + r_- - \sqrt{r_0^2 + z^2})/\rho} + \beta_{c+-} e^{(r_+ + r_- - (r_1 + z))/\rho} + \beta_{c+-} e^{(r_+ + r_- - (r_1 - z))/\rho} \quad (2)$$

where z is the c -axis Fe^{3+} displacement away from the 2b site. The sum of first three terms corresponds to the Coulomb potential U_{Coulomb} between Fe^{3+} and O^{2-} and the sum of

the rest three terms represents the short-range Pauli repulsion potential $U_{\text{repulsion}}$. $(\text{Ba,Sr})\text{Fe}_{12}\text{O}_{19}$ is assumed to be a pure ionic crystal that O ion has $-2e$ charge and Fe ion has $+3e$ charge, e is the electron charge. r_0 and r_1 are the in-plane and out of plane Fe-O distances in the bipyramid for 2b site, obtained from ref. [29] and Table I. β is a constant (taken to be 1.35×10^{-19} J), $c_{+-} = 1$ is Pauling's valence factor, and $\rho = 0.315 \text{ \AA}$ is a parameter derived from the FeO (ref. [28]). $r_+ = 1.4 \text{ \AA}$ and $r_- = 0.58 \text{ \AA}$ are the ionic radii of Fe^{3+} with coordinate number of 5 and O^{2-} with coordinate number of 6, respectively, from ref. [30].

The calculated results are shown in Figs. 3(b)-3(d). Only the $U_{\text{repulsion}}$ terms show the double-well potential feature near $z = 0$ for the parameters we used. The double well in $U_{\text{repulsion}}$ terms becomes smaller and closer with Sr doping while the U_{Coulomb} terms are largely invariant near $z = 0$. Their summation U_{tot} remains the double-well feature, indicating the existence of local electric dipoles in $(\text{Ba,Sr})\text{Fe}_{12}\text{O}_{19}$. In particular, the 4e-4e distances estimated from the simulation decreases systematically from 0.271 to 0.142 \AA by substituting Ba with Sr, which is well consistent with the decreasing tendency of local dipole by Sr doping found in our experiments. Based on above calculations, the short-range Pauli repulsions instead of the Coulomb forces favor the off-equatorial arrangement of Fe^{3+} ion. This is in marked contrast to the case in ABO_3 perovskite ferroelectrics where the long-range Coulomb forces favor the ferroelectric state and short-range repulsions do not. It is very likely due to the unique FeO_5 bipyramid structure as well as the half-filled configuration of Fe^{3+} ($3d^5$).

To provide further insight for the lattice requirements to have the local electric dipoles in FeO₅ bipyramid, we analyzed the extreme conditions of each potential function at $z = 0$. For Coulomb term, to favor off-center displacement of Fe³⁺ ion, it should have $\partial^2 U_{\text{Coulomb}}/\partial z^2|_{z=0} < 0$. One can obtain the corresponding structure requirement: $r_1/r_0 < (4/3)^{1/3} \approx 1.1$. This condition is always unsatisfied for (Ba,Sr)Fe₁₂O₁₉ since $r_1/r_0 > 1.23$ for all the members. For the repulsion term, to have the double-well feature, it should have $\partial^2 U_{\text{repulsion}}/\partial z^2|_{z=0} < 0$. One then obtains the lattice criteria: $e^{r_1/\rho} > 2/3(r_0/\rho e^{r_0/\rho})$. The satisfaction of this criterion depends on the relative magnitude of r_1 and r_0 to ρ , and it happens to be the case for (Ba,Sr)Fe₁₂O₁₉. By combining the conditions of both potential terms, we obtained the phase diagram in the r_1/ρ vs. r_0/ρ plot, as shown in Fig. 3(e). (Ba,Sr)Fe₁₂O₁₉ are found to lie just outside the nonpolar region.

The produced double-well potentials can only guarantee the existence of local dipoles. Nevertheless, to observe quantum paraelectricity, quantum fluctuations must overwhelm the coupling between local dipoles to prevent a ferro or antiferroelectric ordering. A recent first-principle calculation on BaFe₁₂O₁₉ predicted a frustrated antiferroelectric ground state below 3 K [31]. On the contrary, we neither observe in experiments any ferro/antiferroelectric phase transition down to 1.5 K, nor found any trace of long-range ordering in the specific heat data above 2 K. These experimental facts indicate that the previous first-principle calculation could have either ignored the quantum fluctuations or overestimated the dipole-dipole coupling in BaFe₁₂O₁₉. Since the local dipoles are from the FeO₅ bipyramid, the density of dipoles is proportional to the number of FeO₅

bipyramids in the whole lattice. Due to the layered structures, the local dipoles in FeO_5 bipyramids only exist in the R blocks and are separated by the S blocks along c axis. In this case, the coupling between these diluted small dipoles would be quite weak, especially along c axis. Meanwhile, the double-well potentials in $(\text{Ba,Sr})\text{Fe}_{12}\text{O}_{19}$ are very shallow and therefore can be easily disturbed by quantum fluctuations. From above discussions, we conclude that the quantum fluctuations between two opposite off-equatorial configurations overwhelm the weak dipole-dipole coupling and prevent the long-range dipole ordering down to the lowest temperature.

If the local dipoles are really related to the FeO_5 bipyramids within the R blocks, one may expect a similar dielectric behavior in other hexaferrites containing the R blocks. To clarify this point, we further studied a series of available hexaferrites, including Y-type ($\text{BaSrCoZnFe}_{11}\text{AlO}_{22}$) and Z-type ($\text{Ba}_{1.5}\text{Sr}_{1.5}\text{Co}_2\text{Fe}_{24}\text{O}_{41}$) single crystals, and W-type ($\text{BaCo}_2\text{Fe}_{16}\text{O}_{27}$) ceramics. For Y and Z-type hexaferrites, a constant in-plane magnetic field of 5 kOe is applied to stabilize the transverse cone spin configuration below 150 K during the measurements [32,33]. As shown in Figs. 4(a) and 4(b), the W- and Z-type hexaferrites that contain the R blocks indeed shows a sign of quantum paraelectricity, with a similar saturating behavior to that in $(\text{Ba,Sr})\text{Fe}_{12}\text{O}_{19}$. In strong contrast, the Y-type hexaferrite does not show such a saturation behavior. This is exactly consistent with our expectation because Y-type hexaferrites do not contain the FeO_5 bipyramids.

In conclusion, we have disclosed a new mechanism for local electric dipoles based on the FeO_5 bipyramid. As a prototype consequence, this non- d^0 electric dipoles in

hexagonal ferrites (Ba,Sr)Fe₁₂O₁₉ leads to a completely new family of magnetic quantum paraelectrics. More importantly, the significance of the FeO₅ bipyramid goes well beyond quantum paraelectrics only. In principle, a variety of exotic dielectric materials could be expected on the basis of the non- d^0 electric dipole. The amplitude of the electric dipoles and the coupling between them may be enhanced by manipulating the lattice parameters and the density of the bipyramid unit in a designed crystal structure, which may eventually yield unconventional non- d^0 ferroelectrics. Furthermore, the coexistence of both electric dipole and magnetic moment in the FeO₅ bipyramid provides a promising playground for magnetoelectric multiferroics. These topics should deserve further studies in the future.

This work was supported by the Natural Science Foundation of China under Grant Nos. 11227405 and 11374347, the National Key Basic Research Program of China under Grant No. 2011CB921801, and the China-Israel joint project under Grant No. 2013DFG13020.

References

- [1] R. E. Cohen, *Nature* **358**, 136 (1992).
- [2] R. E. Cohen and H. Krakauer, *Ferroelectrics* **136**, 65 (1992).
- [3] B. T. Matthias, *Phys. Rev.* **75**, 1771 (1949).
- [4] N. A. Hill, *J. Phys. Chem. B* **104**, 6694 (2000).
- [5] R. Seshadri and N. A. Hill, *Chem. Mater.* **13**, 2892 (2001).
- [6] S.-W. Cheong and M. Mostovoy, *Nature Mater.* **6**, 13 (2007).
- [7] N. Ikeda *et al.*, *Nature* **436**, 1136 (2005).
- [8] Y. Sun, L.-Q. Yan, and J.-Z. Cong, *Sci. China-Phys. Mech. Astron.* **56**, 222 (2013).
- [9] B. B. van Aken *et al.*, *Nature Mater.* **3**, 164 (2004).
- [10] S. Bhattacharjee *et al.*, *Phys. Rev. Lett.* **102**, 117602 (2009).
- [11] J. M. Rondinelli *et al.*, *Phys. Rev. B* **79**, 205119 (2009).
- [12] J. H. Lee and K. M. Rabe, *Phys. Rev. Lett.* **104**, 207204 (2010).
- [13] H. Sakai *et al.*, *Phys. Rev. Lett.* **107**, 137601 (2011).
- [14] P. B. Braun, *Phillips Res. Rep.* **12**, 491 (1957).
- [15] J. A. Kohn, D. W. Eckart, and C. F. Jr Cook, *Science* **172**, 519 (1971).
- [16] J. Smit and H. P. J. Wijn, *Ferrites* (Phillips Technical Library, 1959).
- [17] Z. F. Zi *et al.*, *J. Magn. Magn. Mater.* **320**, 2746 (2008).
- [18] See Supplemental Material for the details of sample preparation, characterization, and heat capacity.
- [19] K. A. Müller and H. Burkhard, *Phys. Rev. B* **19**, 3593 (1979).

- [20] V. V. Lemanov, A. V. Sotnikov, and E. P. Smirnova, *Solid State Commun.* **110**, 611 (1999).
- [21] A. R. Akbarzadeh *et al.*, *Phys. Rev. B* **70**, 054103 (2004).
- [22] J. H. Barret, *Phys. Rev.* **86**, 118120 (1952).
- [23] T. Katsufuji and H. Takagi, *Phys. Rev. B* **64**, 054415 (2001).
- [24] X. Obradors *et al.*, *J. Solid State Chem.* **56**, 171 (1985).
- [25] J. G. Rensen, and J. G. van Wieringen, *Solid State Commun.* **7**, 1139 (1969).
- [26] X. Obradors *et al.*, *Solid State Chem.* **72**, 218 (1988).
- [27] G. Albanses, A. Deriu, and D. Cabrini, *Hyperfine Interactions* **70**, 1087 (1992).
- [28] S. P. Marshall and J. B. Sokoloff, *Phys. Rev. B* **44**, 619 (1991).
- [29] O. P. Aleshko-Ozhevskii, M. K. Faek, and I. I. Yamzin, *Soviet Physics-Cryst.* **14**, 447 (1969).
- [30] R. D. Shannon, *Acta Cryst.* **A32**, 751 (1976).
- [31] P. S. Wang and H. J. Xiang, *Phys. Rev. X* **4**, 011035 (2014).
- [32] S.-P. Shen *et al.*, *Appl. Phys. Lett.* **104**, 032905 (2014).
- [33] M. Soda *et al.*, *Phys. Rev. Lett.* **106**, 087201 (2011).

Figure captions

FIG. 1 (color online). Crystal structures of M, Y, W, and Z-type hexaferrites.

FIG. 2 (color online). The c -axis dielectric permittivity ϵ_c as a function of temperature for (a) $\text{BaFe}_{12}\text{O}_{19}$, (c) $\text{Ba}_{0.5}\text{Sr}_{0.5}\text{Fe}_{12}\text{O}_{19}$, and (d) $\text{SrFe}_{12}\text{O}_{19}$. (b) The ab -plane dielectric permittivity ϵ_{ab} for $\text{BaFe}_{12}\text{O}_{19}$. The black solid lines are the fitting curves to Eq. (1). The insets are the same plots with a logarithmic scale in temperature.

FIG. 3 (color online). (a) Schematic illustration of Fe^{3+} off-equatorial displacements in the FeO_5 bipyramid. The up and down displacements correspond to two $4e$ sites with opposite dipoles and local minimums in energy potential. The calculated energy potentials from Eq. (2) for (b) U_{Coulomb} , (c) $U_{\text{repulsion}}$, and (d) the sum U_{tot} as a function of off-equatorial Fe^{3+} displacement z in $(\text{Ba,Sr})\text{Fe}_{12}\text{O}_{19}$. (e) Phase diagram to allow the double-well potential. In the central yellow region, the double-well potential is not allowed. In the left corner, it must appear. In the rest regions, it is possible due to the competition between the Coulomb attraction and Pauli repulsion.

FIG. 4 (color online). The temperature dependent dielectric permittivity of (a) the W-type hexaferrite $\text{BaCo}_2\text{Fe}_{16}\text{O}_{27}$ ceramic, (b) the Z-type hexaferrite $\text{Ba}_{1.5}\text{Sr}_{1.5}\text{Co}_2\text{Fe}_{24}\text{O}_{41}$ single crystal along c axis, and (c) the Y-type hexaferrite $\text{BaSrCoZnFe}_{11}\text{AlO}_{22}$ single crystal along c axis.

Table I. The fitting parameters T_0 , T_1 and M to Eq. (1). The values in bold are not reliable. The Fe-O bond lengths in the FeO_5 bipyramid for $\text{BaFe}_{12}\text{O}_{19}$ and $\text{SrFe}_{12}\text{O}_{19}$ at room temperature are derived from ref. [29]. The bond lengths of $\text{Ba}_{0.5}\text{Sr}_{0.5}\text{Fe}_{12}\text{O}_{19}$ are linearly extrapolated from that of the end members.

$\text{Ba}_{1-x}\text{Sr}_x\text{Fe}_{12}\text{O}_{19}$	$x = 0.0$	$x = 0.5$	$x = 1.0$
T_0 (K)	-11.7	-9.7	53.1
T_1 (K)	54.9	67.6	130.6
M (K)	452	224	7.4
Fe- O_{ap} (Å)	2.325	2.315	2.305
Fe- O_{ab} (Å)	1.870	1.8665	1.863

Figure 1

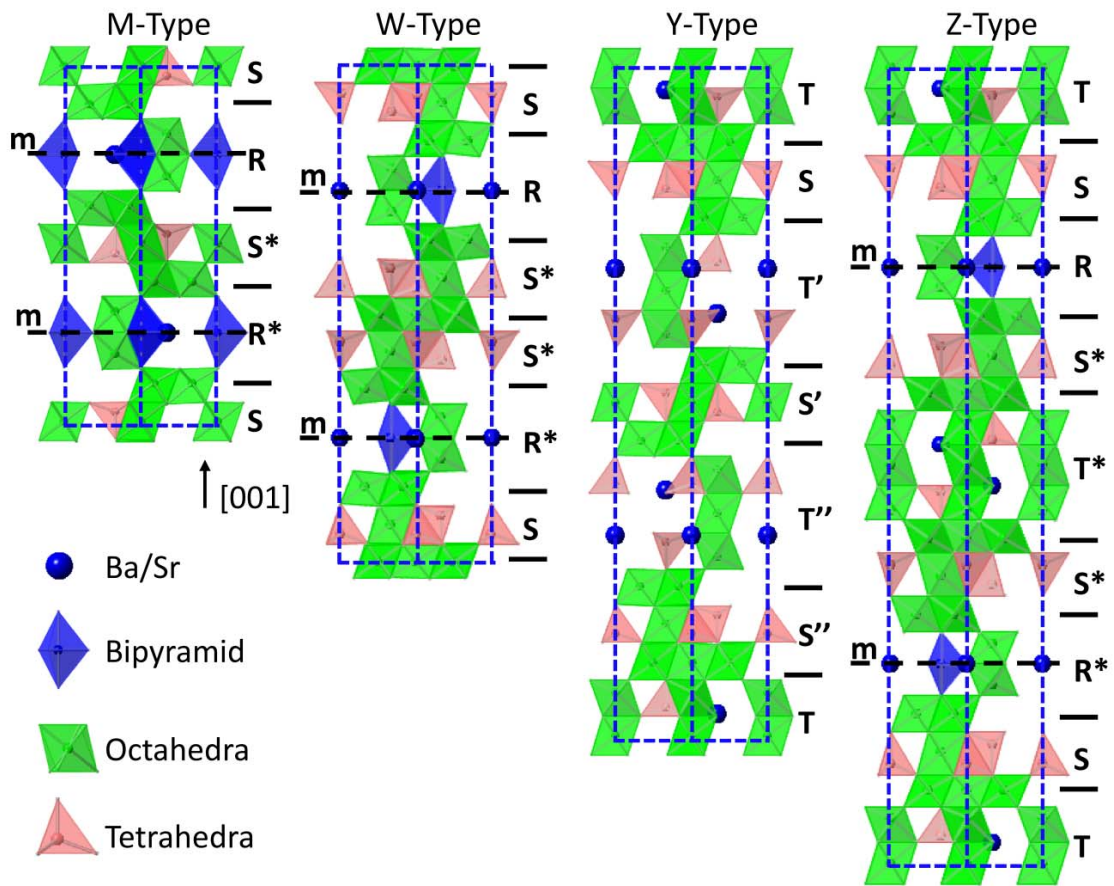


Figure 2

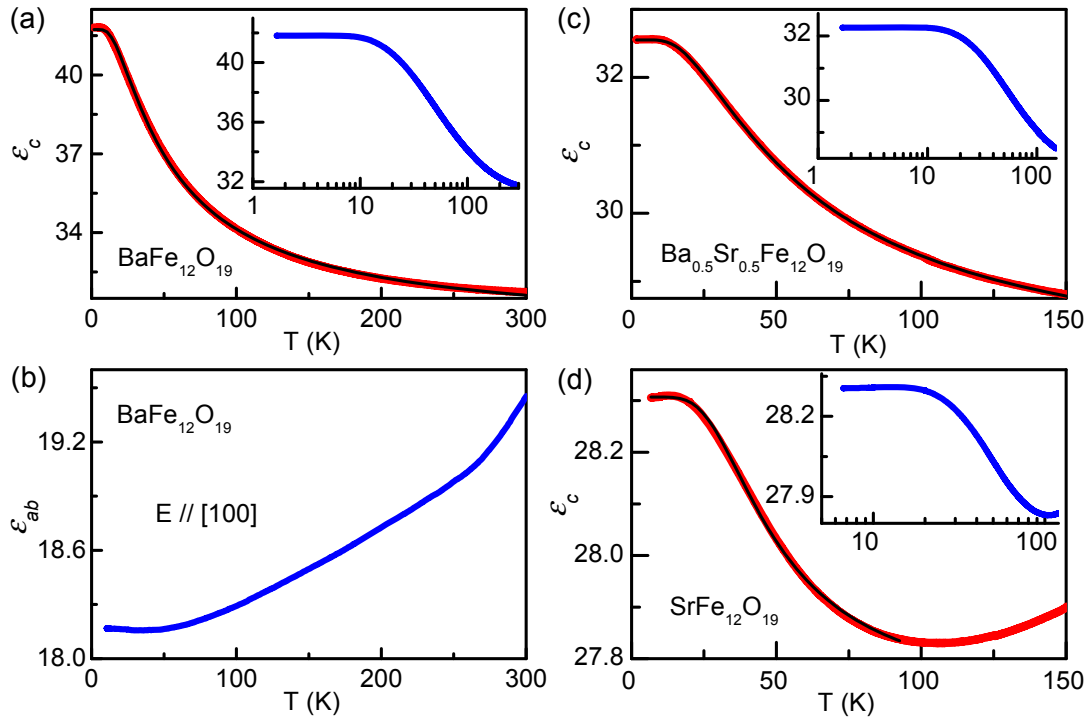


Figure 3

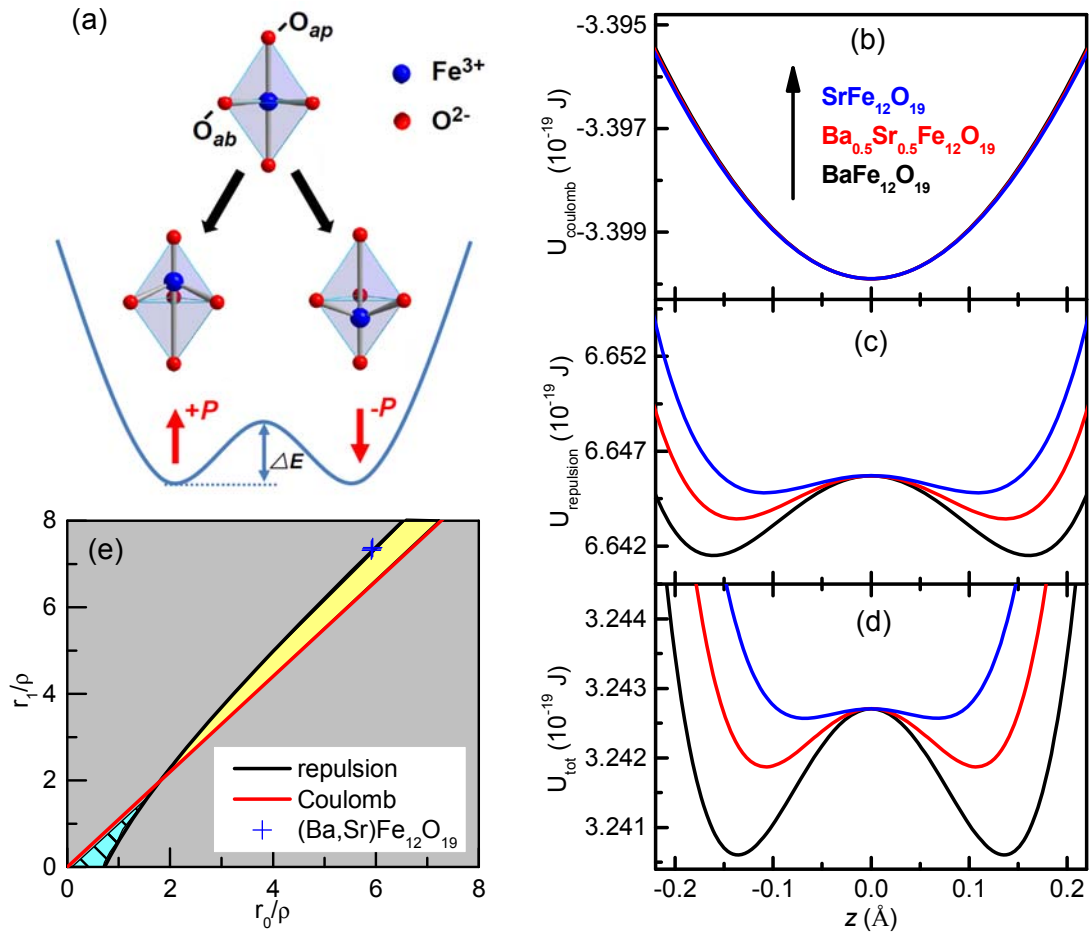


Figure 4

